



D2.1 Functionalised platform materials by exsolution

Project Information	
Title	From solar energy to fuel: A holistic artificial photosynthesis platform for the production of viable solar fuels
Acronym	REFINE
Project Call	HORIZON-CL5-2022-D3-03
Project Topic	HORIZON-CL5-2022-D3-03-03
Grant Agreement ID	101122323
Project Duration	48 months: 1st November 2023 – 31st October 2027

Document Information	
Contractual Date of Delivery	M12
Actual Date of Delivery	M12
Author(s)	Dragos Neagu, Ubong Essien, Adaora Ekperechukwu, Micah Soriano, Kimia Jafari, Alexander Sands, Athanasios Chatzitakis, Sarah Geo, Henrik Petlund, Klaudia Kawucha, Malgorzata Skorupska
Lead Participant	UoS
Contributing Participant(s)	UiO
Work Package(s)	WP2
Dissemination Level (PU/SEN)	PU
Nature (R/DEC/DEM/DMP)	R
Version	1.3







Document History

Version	Issue Date	Changes	
[1.0]	27.10.2024		
[1.1]	29.10.2024	Added content for section on STFM materials for OER and integrated with the other sections.	
[1.2]	30.10.2024	Final version	
[1.3]	11.11.2024	Revised version. Added disclaimer text on page 13	





Table of Contents

_	Conclusions	
4	ELECTROCHEMICAL CHARACTERIZATION OF THE SYNTHESIZED BSCF- AND STFN-BASED CATALYS 11	TS
3	OER CATALYST MATERIALS BASED ON SR _{1-A} (Ti,FE,M)O ₃ (STFM)	7
2	OER CATALYST MATERIALS BASED ON BA _{0.5} SR _{0.5} CO _{0.8} FE _{0.2} O _{3-Δ} (BSCF)	. 2
1	SUMMARY AND SCOPE	2





1 Summary and scope

The main scope of this deliverable is to present the first Stage of catalyst materials for the oxygen evolution reaction (OER) in alkaline environment that will be employed as anodes in Unit 1 (solar-driven alkaline electrolyzer). The Stage 1 platform materials includes the synthesis and characterization of: i) $Ba_{0.5}Sr_{0.5}Co_{0.8}Fe_{0.2}O_{3-\delta}$ -based catalysts (BSCF) and their derivatives with reduced cobalt (Co) contents, and ii) $Sr_{1-a}(Ti,Fe,M)O_3$ (STFM, M =Fe, Cu, Ni) with no Co. Nevertheless, and for benchmarking purposes, STFNs with low Co contents will also be synthesized. The design of these catalysts is done by using defect chemistry principles, forming a series of 3-5 members each, to promote exsolution. The systems will then be prepared and characterised compositionally, structurally and electrochemically as benchmarks.

The targeted performance of these catalysts by the end of the project is that they can deliver 50 mA/cm² at an overpotential of 400 mV, i.e. at 1.63 V vs the reversible hydrogen electrode (RHE). Their stability should reach at least 2000 h at near-neutral or alkaline pH. Moreover, a key aim is to minimize or even completely deplete cobalt (Co), but also minimize the amounts of precious metals like iridium (Ir) and ruthenium (Ru). The latter will be introduced during Stage 3 of catalysts developments in REFINE.

2 OER catalyst materials based on Ba_{0.5}Sr_{0.5}Co_{0.8}Fe_{0.2}O_{3-δ} (BSCF)

The BSCF-based catalysts were synthesized by the sol-gel citrate method in which the nitrate precursors and barium carbonate (BaCO₃) are mixed and treated in order to form a gel, which is combusted at 250°C. The obtained ash is then fired at 450°C and finally calcined at 1100°C. The main synthetic steps are given in Figure 1.

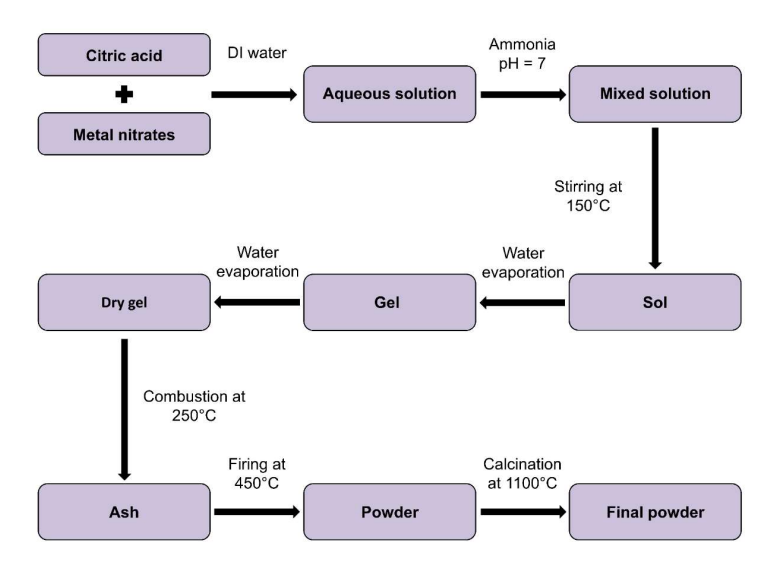


Figure 1: Synthesis steps of the sol-gel citrate method used to synthesize the BSCF-based catalysts.

By following this methodology, we have currently synthesized the following compositions, where a reduction in the Co content has been implemented.

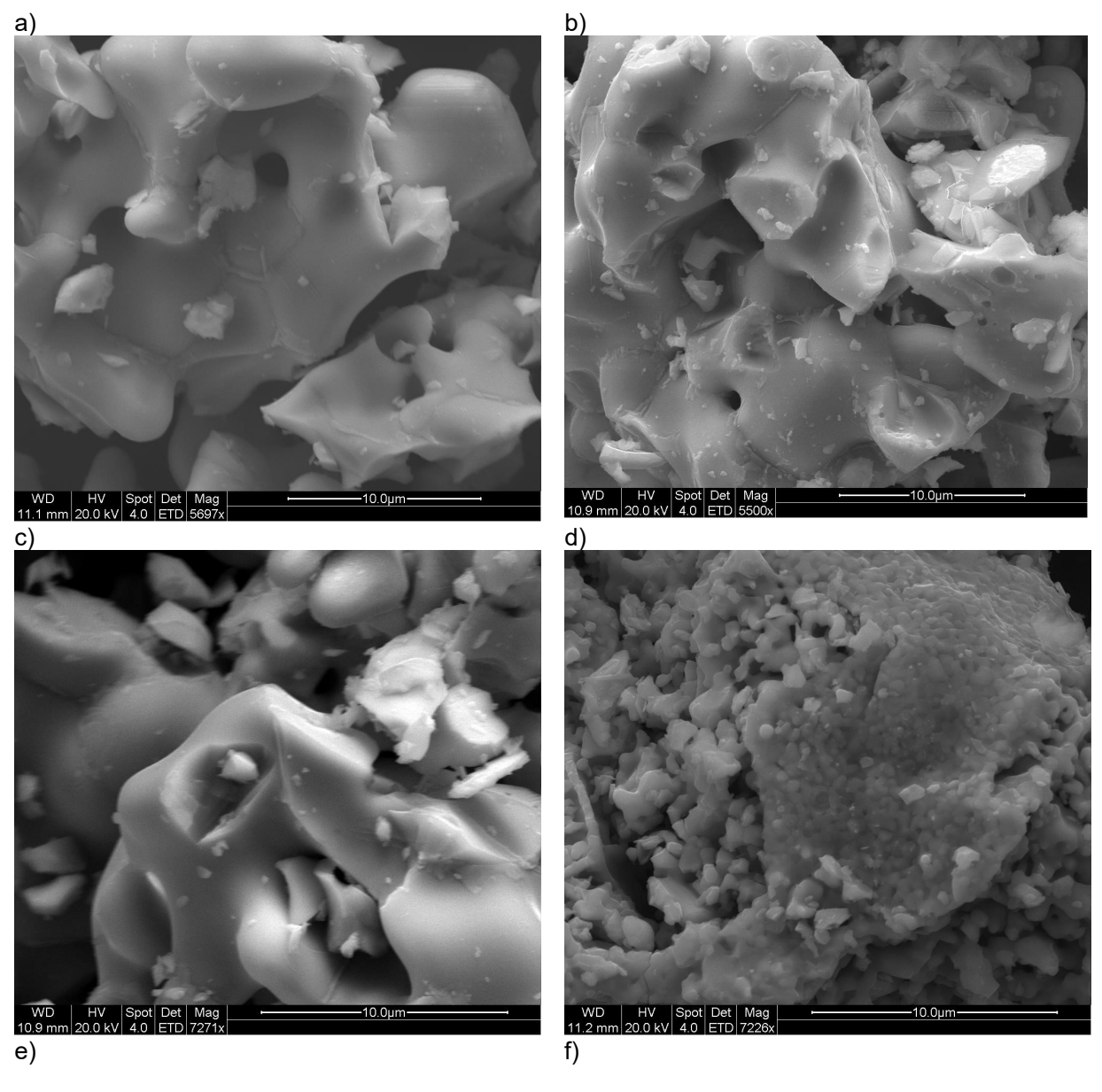




Table 1: Composition of the BSCF-based catalysts designed and synthesized with their respective abbreviations and nominal B-site substitution

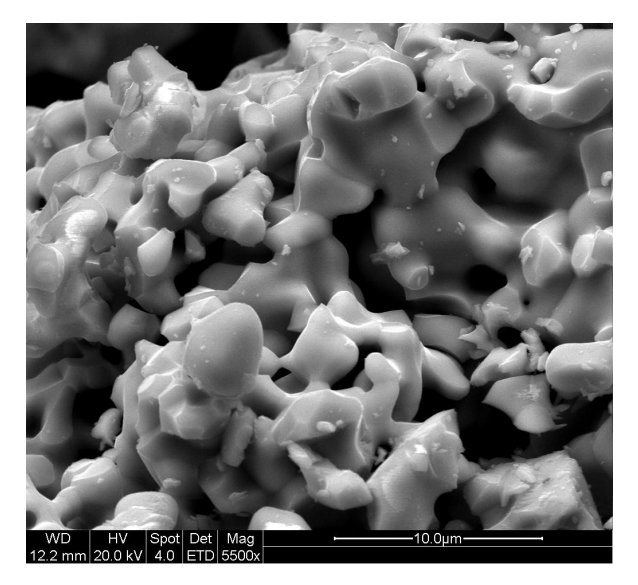
Stoichiometric composition	Abbreviation	Nominal substitution / comment
Ba _{0.5} Sr _{0.5} Co _{0.8} Fe _{0.2} O _{3-δ}	BSCF82	Base material, B-site: 20% Fe
Ba _{0.45} Sr _{0.45} Co _{0.8} Fe _{0.2} O _{3-δ}	BSCF82-10AD	10% A-site deficiency, B-site: 20% Fe
Ba _{0.475} Sr _{0.475} Co _{0.8} Fe _{0.2} O _{3-δ}	BSCF82-5AD	5% A-site deficiency, B-site: 20% Fe
Ba _{0.475} Sr _{0.475} Co _{0.8} Fe _{0.2} O _{3-δ}	BSCF82-5AD	5% A-site deficiency, B-site: 20% Fe / annealed at 900 °C
Ba _{0.5} Sr _{0.5} Co _{0.6} Fe _{0.4} O _{3-δ}	BSCF64	B-site: 40% Fe
$Ba_{0.475}Sr_{0.475}Co_{0.6}Fe_{0.4}O_{3-\delta}$	BSCF64-5AD	5% A-site deficiency, B-site: 40% Fe

All BSCF-based catalysts have been characterized by scanning electron microscopy (SEM) and X-ray diffraction (XRD) in order to observe and verify their structure and crystallinity. The SEM and XRD results are given below.









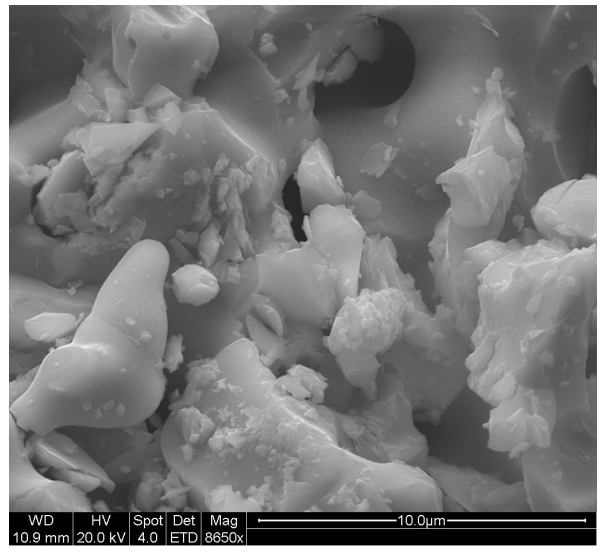
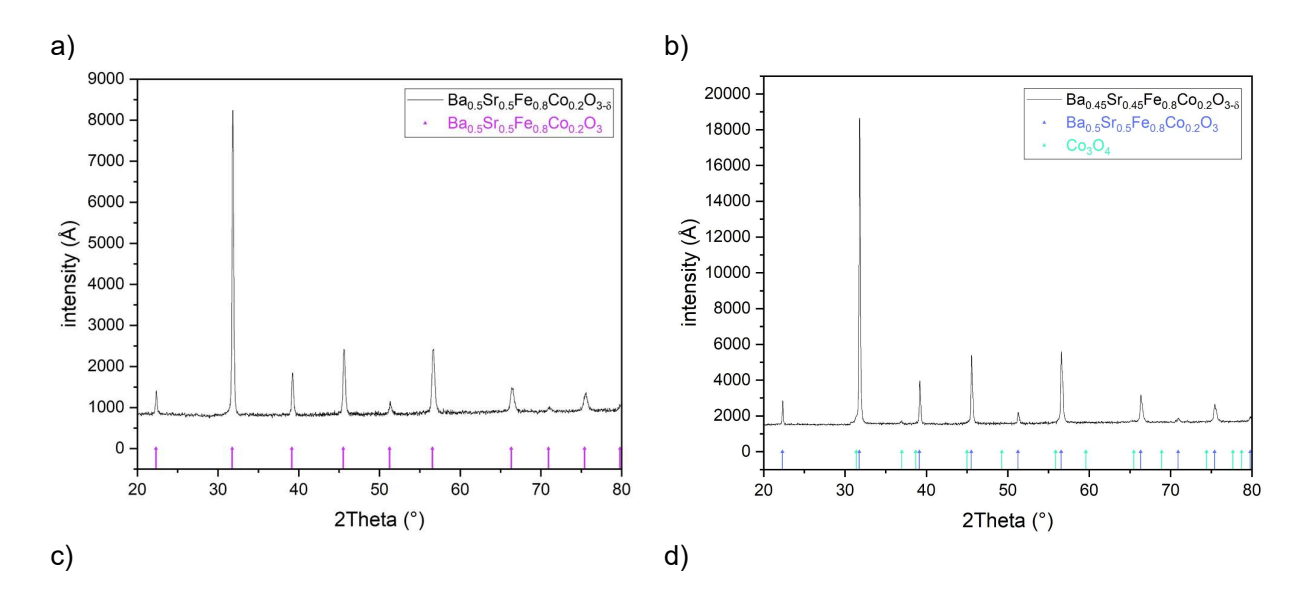


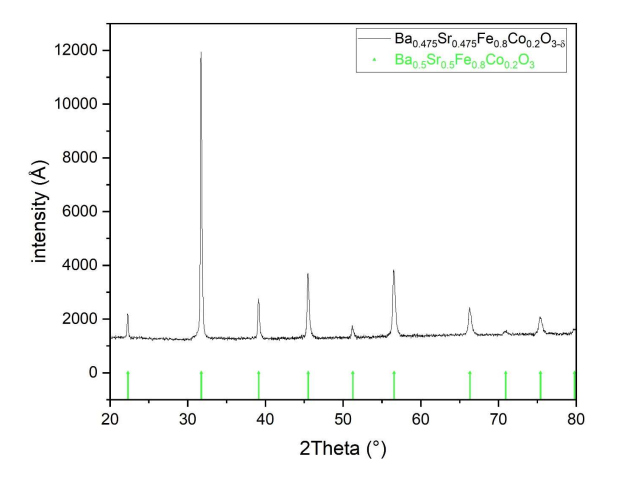
Figure 2: SEM images of a) BSCF82, b) BSCF82-10AD, c) BSCF82-5AD, d) BSCF82-5AD annealed at 900°C, e) BSCF64, f) BSCF64-5AD.

All BSCF82-based catalysts appear to have the same granular morphology with grain sizes in the range of a few micrometers, with the exception of BSCF82-5AD that was annealed at 900° C. As the annealing temperature was lowered, it was expected that the grain sizes would decrease, and appear to be in the range of 1 μ m. Lowering the Co content in BSCF64 it also appears to decrease somewhat the grain sizes, but they are still in the range of a few μ m. The XRD diffractograms are presented in Figure 3.









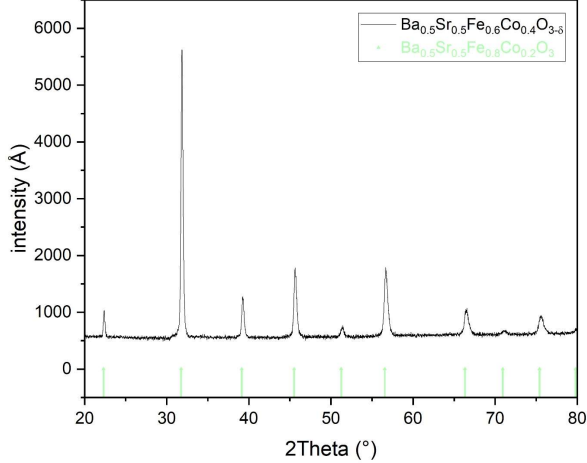
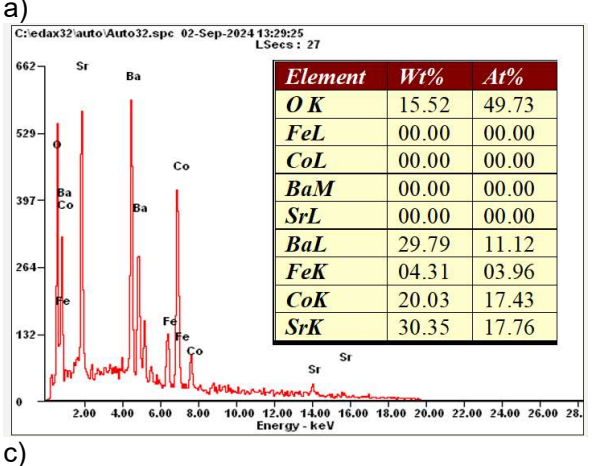
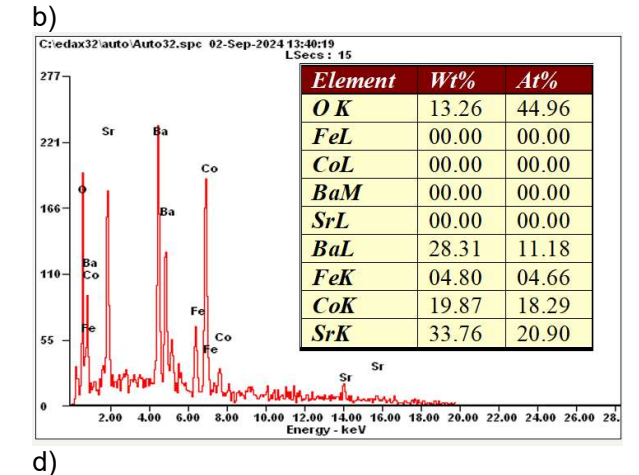


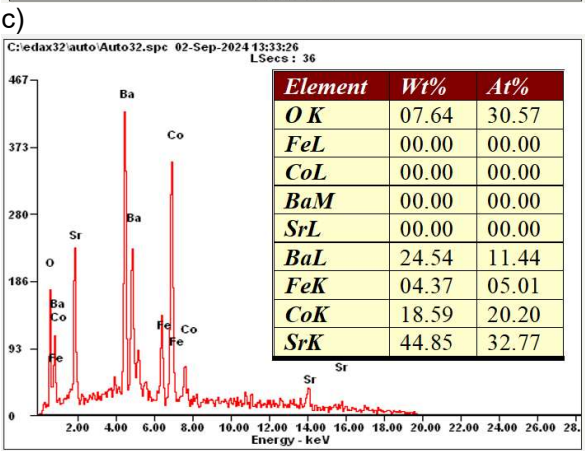
Figure 3: XRD diffractograms of a) BSCF82, b) BSCF82-10AD, c) BSCF82-5AD and d) BSCF64.

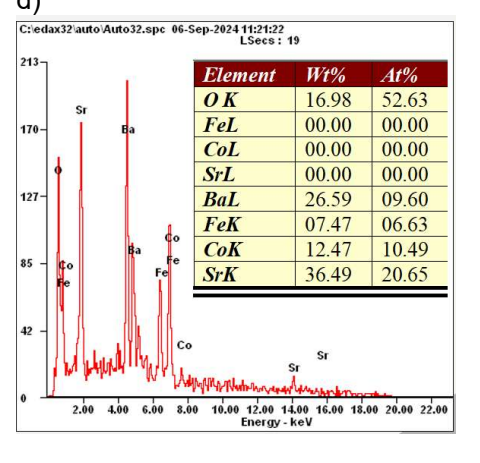
The XRD patterns of BSCF82-5AD that was annealed at 900 °C and of BSCF64-5AD are identical to BSCF82-5AD annealed at 1100°C (c) and BSCF64 (d), respectively. The XRD patterns confirm the successful synthesis of all the samples, as well as their high degree of crystallinity. All samples appear to be single phase except for a small amount of a secondary phase of Co_3O_4 in BSCF82-10AD.

Finally, the elemental composition of the BSCF-based catalysts was studied by energy dispersive spectroscopy (EDS). The results are given in Figure 4.















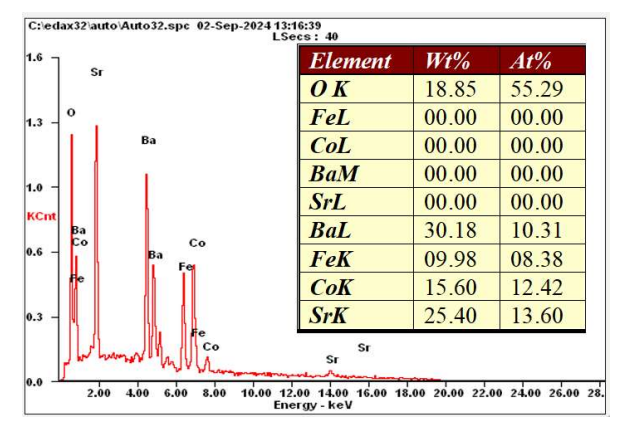


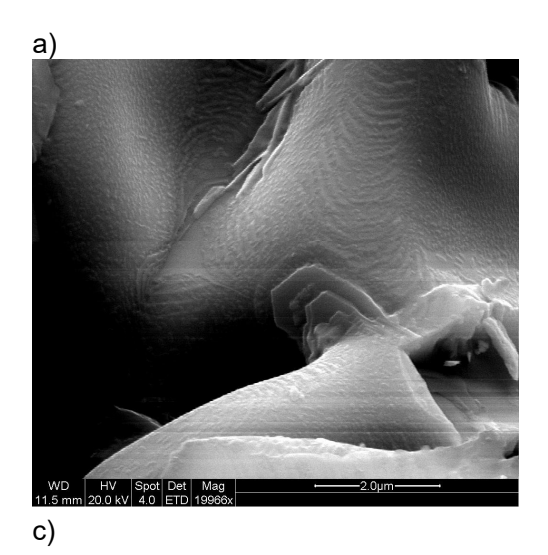
Figure 4: EDS spectra of a) BSCF82, b) BSCF82-10AD, c) BSCF82-5AD, d) BSCF64, e) BSCF64-5AD

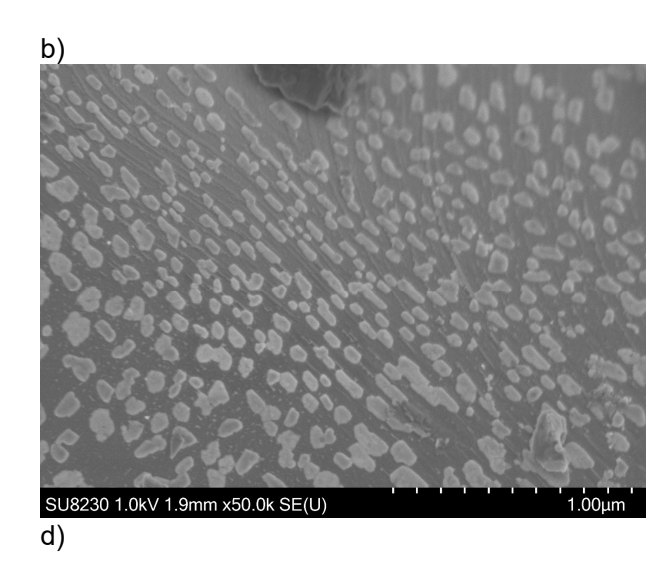
The EDS analysis shows that the samples do not contain any impurities and all the expected elements are present (Ba, Sr, Co and Fe). It is important to notice that the Co/Fe atomic weight precent (At%) ratio correlates well with the expected ratio from the nominal compositions in BSCF82 (4/1) and BSCF64 (3/2). This further showcases the successful synthesis of the different BSCF-based catalysts.

The A-site deficiency is important in order to engineer the materials for exsolution of the B-site cations, according to the following equations.

$$ABO_{3-\delta} \xrightarrow{exsolution} (1-a)ABO_{3-\delta} + aAO + aB \text{ (reducing conditions)}$$
 Eq. 1
$$A_{1-a}BO_{3-\delta lim} \xrightarrow{exsolution} (1-a)ABO_{3-\delta} + aB \text{ (reducing conditions)}$$
 Eq. 2

Currently, we have treated under reducing conditions (5% H_2 in Ar (HArmix), at 700°C for 1 h) the BSCF82-5AD and the microstructure changes as seen below.









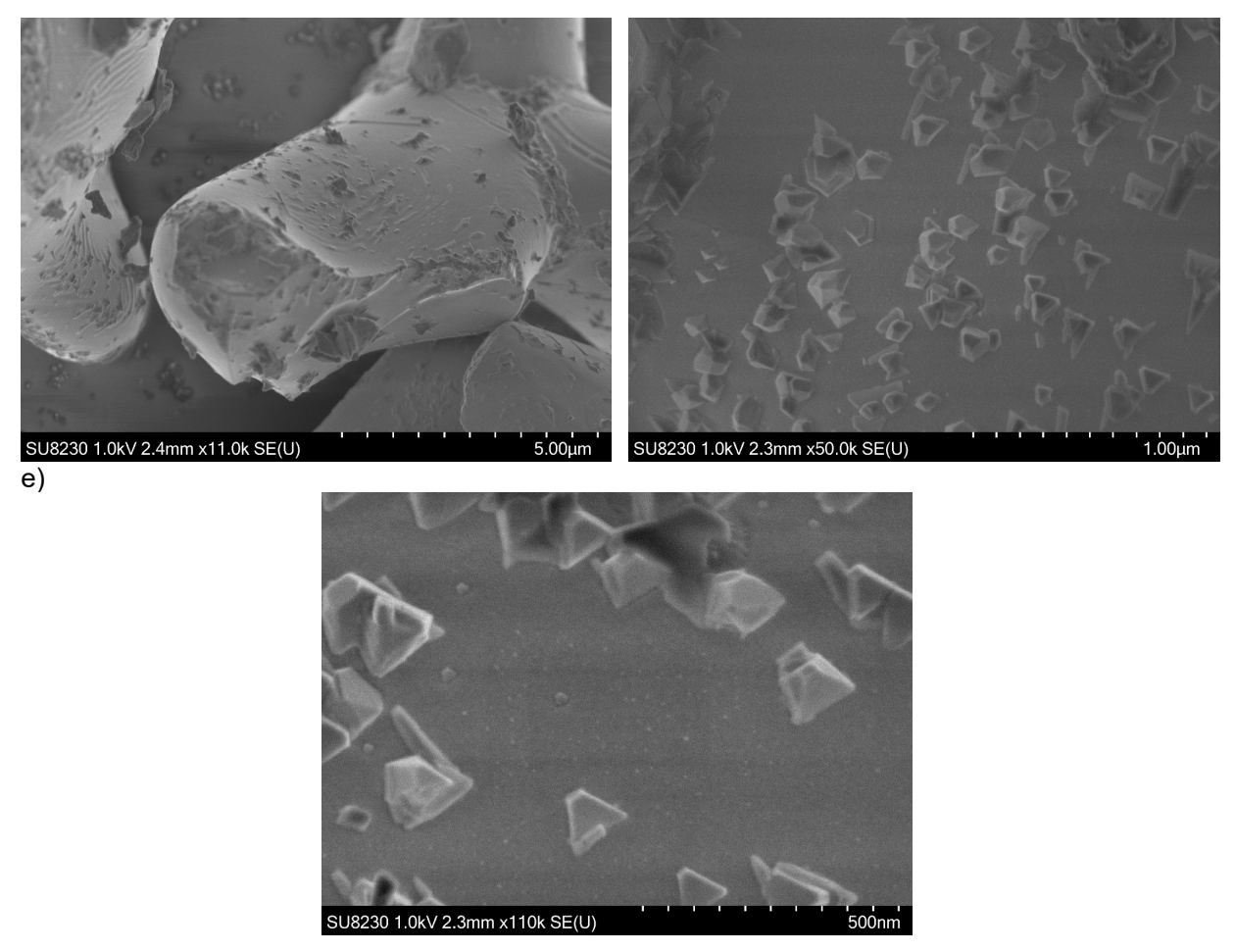


Figure 5: SEM images of BSCF82-5AD a) before exsolution, b) higher magnification of a), c) after exsolution at 700°C for 1 h in HArmix, d) and e) higher magnification images of c).

The change in the surface morphology before and after the exsolution process is obvious. Before exsolution, the surface of BSCF82-5AD is covered by islands of a secondary phase, which could well correspond to Co_3O_4 , as it has been observed by XRD (see Figure 3b). After exsolution, we observe the appearance of small nanoparticles (in the range of a few nanometers – see Figure 5e), as well as larger, highly crystalline and faceted deposits, which are in the range of 100 nm. Both materials are currently under further physicochemical characterization.

3 OER catalyst materials based on Sr_{1-a}(Ti,Fe,M)O₃ (STFM)

The STFM-based catalysts were synthesized using a modified solid-state method. The process began with conditioning of precursor materials (oxides, carbonates, and nitrates), which were dried at temperatures between 300-800°C to remove moisture. A homogeneous mixture was achieved by combining the dried precursors with acetone and approximately 0.05 wt.% Hypermer KD-1 dispersant (polyester/polyamide copolymer). The resulting slurry underwent ultrasonic treatment to break down agglomerates and achieve improved particle dispersion. The mixture was then continuously dried and stirred to maintain homogeneity as the acetone evaporated.

The homogenized precursor mixture was calcined at 1000°C for 12 hours to facilitate carbonate decomposition and initiate perovskite phase formation. Post-calcination yields were satisfactory,



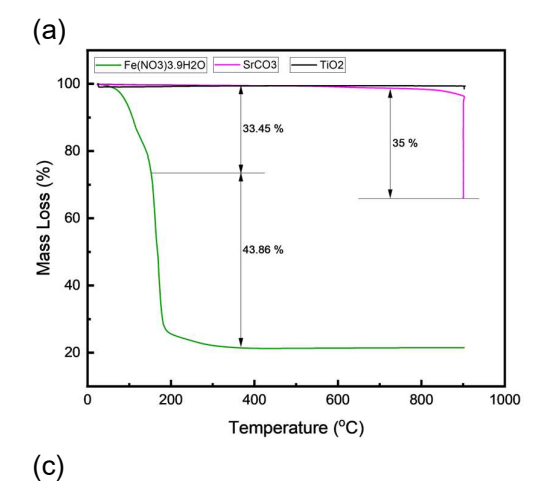


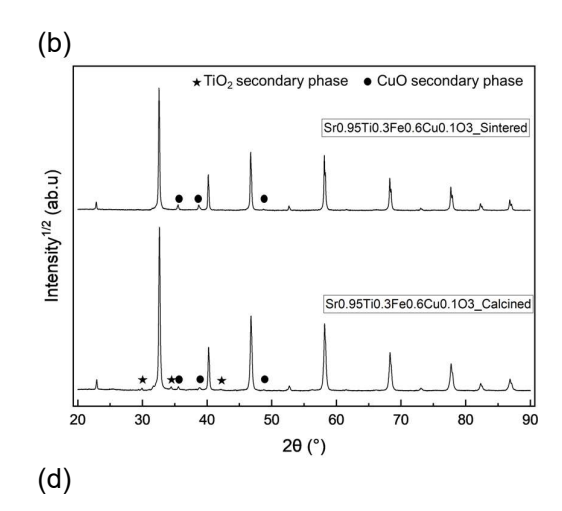
achieving over 99% of the target mass. The calcined powders were then compressed into dense pellets and sintered at temperatures between 1000-1150°C for 12 hours, with specific temperatures selected based on composition. This final sintering step ensured complete densification and development of the desired perovskite phase structure.

Table 2: Composition of the STFN-based catalysts designed and synthesized with their respective abbreviations and nominal B-site substitution

Stoichiometric composition	Abbreviation	Nominal substitution / comment
$Sr_{0.95}Ti_{0.3}Fe_{0.7}O_3-\gamma$	Sr95TF3070	5% A-site deficiency, B-site: 30% Ti, 70% Fe
$Sr_{0.95}Ti_{0.3}Fe_{0.6}Cu_{0.1}O_3-\gamma$	Sr95TFC306010	5% A-site deficiency, B-site: 30% Ti, 60% Fe, 10% Cu
$Sr_{0.95}Ti_{0.3}Fe_{0.6}Ni_{0.1}O_{3}$ - γ	Sr95TFN306010	5% A-site deficiency, B-site: 30% Ti, 60% Fe, 10% Ni

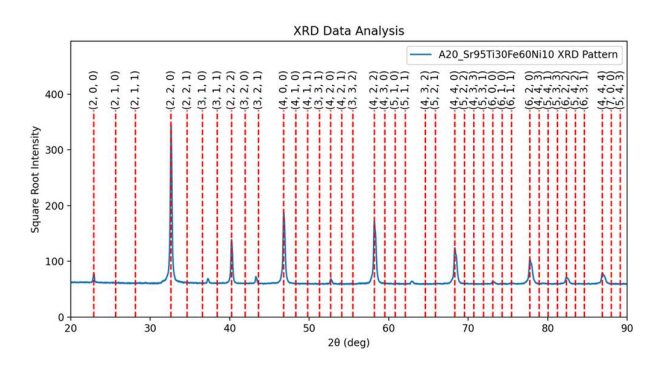
Some key results are highlighted in Figure 6. Thermal analysis of the precursors (Figure 6a) reveals distinct decomposition steps, with Fe(NO₃)₃·9H₂O showing a sharp mass loss by 200°C due to dehydration and nitrate decomposition, while SrCO₃ exhibits a mass loss around 800°C corresponding to carbonate decomposition. This justifies the selection of calcination temperature in excess of these values, by 1000°C. XRD analysis confirms the formation of the primary perovskite phase in all compositions, with some secondary phases of TiO₂ and CuO detected in the Cu-substituted variant. The sintering step at 1000-1150°C notably reduces these secondary phases, as evidenced by the comparative diffraction patterns (Figure 6b). Figure 6c illustrates the procedure used to identify the space group associated with the synthesised perovskite, by indexing on a double cubic cell and analysing Miller indices to identify sublattice type reflections. Rietveld refinement of the final structure indicates good agreement between observed and calculated patterns, confirming the successful synthesis of the target perovskite phases (Figure 6d). A minor CuO secondary phase is still observed and quantified in the model. Such analysis was carried out for all synthesised samples.











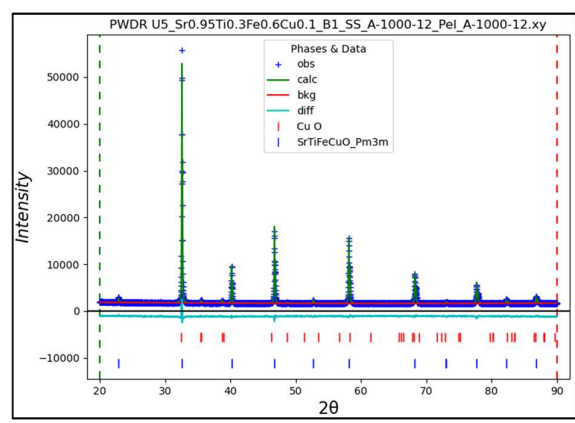


Figure 6: STFM materials, from precursors to phase formation and analysis. (a) TGA curves showing mass loss behaviour of the precursors $Fe(NO_3)_3 \cdot 9H_2O$, $SrCO_3$, and TiO_2 ; (b) XRD patterns of Sr95FTC306010 after calcination and sintering, showing secondary phases (*: TiO_2 , •: CuO); (c) XRD pattern with peak indexing for the Sr95TFN306010 composition; (d) Rietveld refinement of the Sr95FTC306010 structure showing observed data (crosses), calculated pattern (green line), difference plot (cyan), and Bragg positions (red tick marks).

The SEM analysis reveals distinct microstructural features between the base and Cu-substituted compositions (Figure 7). The Sr95TF3070 sample displays a characteristic interconnected network of grains with uniform porosity and grain sizes ranging from ~0.2-1.5 µm, while the Cu-containing Sr95TFC306010 exhibits notably different grain morphology with evidence of enhanced sintering and larger grain sizes between ~0.5-3 µm. This microstructural evolution suggests that Cu incorporation promotes densification and affects the grain boundary development during the sintering process, resulting in significant grain growth. Sr95TFN306010 exhibited even more significant grain growth, albeit, it was sintered at a higher temperature. The increased grain size will lead to decreased surface area which is expected to lower available electrocatalytic area, and therefore limit electrocatalytic activity.

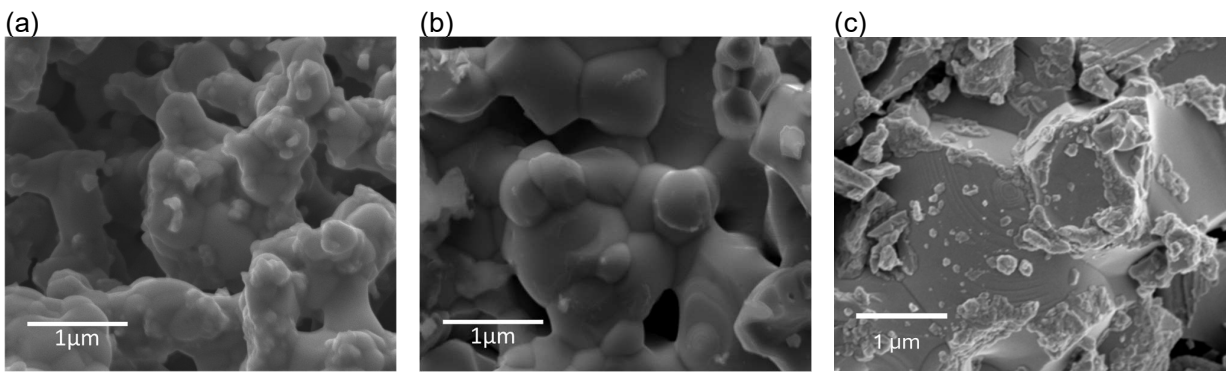


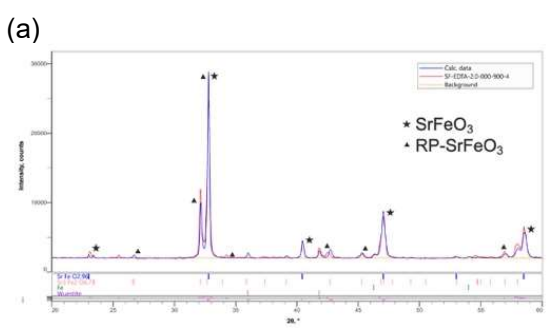
Figure 7: SEM micrographs of sintered STFM-based materials showing surface morphology: (a) Sr95TF3070 exhibiting interconnected porous structure (1000°C, 12 h); (b) Sr95TFC306010 showing modified grain morphology and enhanced densification due to Cu incorporation (1000°C, 12 h). (c) Sr95TFN306010 showing significant grain growth and a certain level of faceting (1150°C, 12 h).

To address this limitation, alternative synthetic routes that avoid high-temperature sintering are being explored to maximize the catalytic activity through higher surface area materials. Several methods have been investigated, including combustion synthesis, hydrothermal, and sol-gel approaches (see preliminary XRD results in Figure 8). The combustion synthesis, utilizing various fuels (citric acid, EDTA, glycine, and urea) at different ratios, has shown promising results with the potential formation of oxygen-





deficient phases ($Sr_nFe_nO_{3n-1}$) not accessible via conventional solid-state synthesis, despite some remaining secondary phases. Among the soft-chemistry approaches, sol-gel synthesis has proven more effective than hydrothermal methods in achieving the desired perovskite structure. While hydrothermal synthesis predominantly resulted in oxide phases (anatase, rutile, magnetite, and hematite), the sol-gel method consistently produced the target perovskite structure with relatively fewer secondary phases.



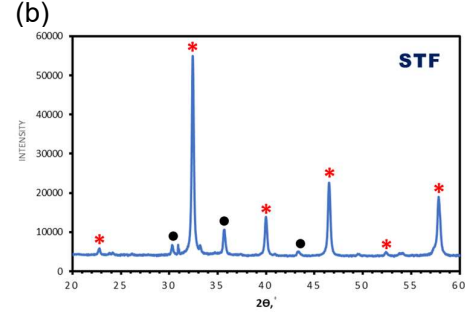
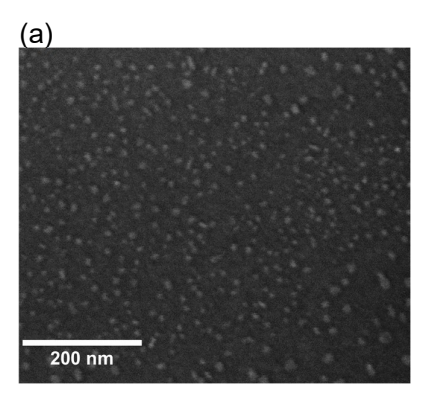
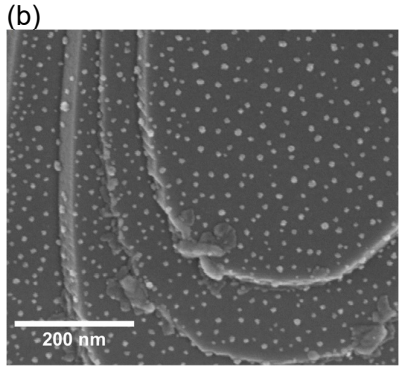


Figure 8: XRD analysis of STF-type perovskite compositions prepared by various methods, after calcination at 800-900°C (a) combustion method showing initial assignment of perovskite type phases, potentially including $Sr_nFe_nO_{3n-1}$ type structures and (b) sol-gel method showing main perovskite phase (red) alongside magnetite secondary phase (blue).

Reduction treatments were conducted on the synthesized materials to initiate exsolution of B-site cations and thus formation of surface nanoparticles with electrocatalytic activity. The samples were exposed to reducing conditions at temperatures of 400°C and 600°C for durations ranging from 1 to 3 hours. These parameters were found to be critical in controlling both the size and population density of exsolved nanoparticles on the surface. The ability to tune the reduction temperature and time provides a valuable pathway for future optimization, allowing control over the exsolved particle characteristics to enhance catalytic performance.

The exsolution process resulted in distinctly different nanostructures across the three compositions (Figure 9). The base Sr95TF3070 material exhibits a high population density of uniformly distributed fine particles with an average size of ~10 nm after 3 hours of reduction. In contrast, the Cu-substituted variant (Sr95TFC306010) developed larger particles (~25 nm) with a more regular spherical morphology after just 1 hour of reduction, suggesting enhanced exsolution kinetics. The Ni-containing composition (Sr95TFN306010) produced the largest particles (~40 nm) and uniform distribution across the porous perovskite framework. These observations demonstrate how compositional variations significantly influence both the exsolution kinetics and resulting particle characteristics.





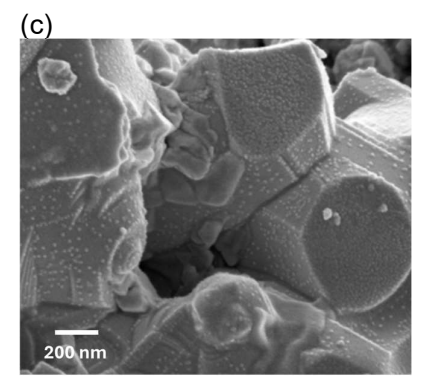


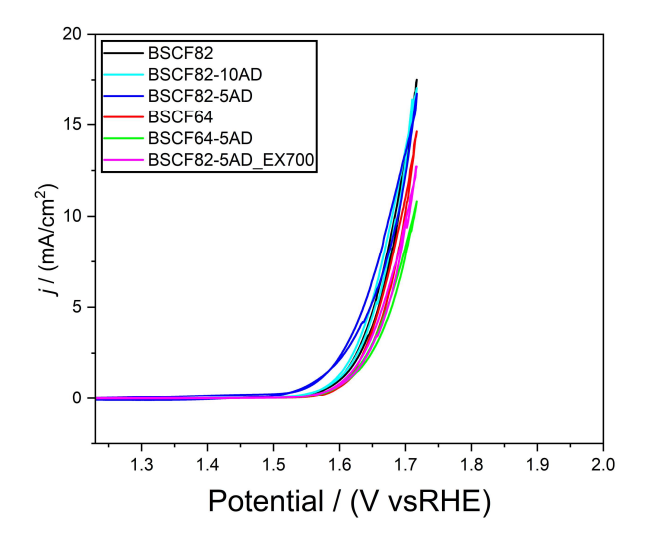


Figure 9: SEM micrographs showing exsolved nanoparticles after reduction at 600°C: (a) Sr95TF3070 after 3 hours showing uniformly distributed fine particles; (b) Sr95TFC306010 after 1 hour displaying well-defined particles with increased size; (c) Sr95TFN306010 after 1 hour exhibiting larger particles with distinctive morphology. Scale bars: 200 nm.

4 Electrochemical characterization of the synthesized BSCF- and STFN-based catalysts

After confirming the successful synthesis of both types of catalyst materials developed in REFINE for the anode side and OER in Unit 1, we are currently performing their electrochemical characterization. Cyclic voltammetry (CV) and linear sweep voltammetry (LSV) have been used as the first activity indicator and the results of a first set of catalysts are presented in Figure 10.

a)



b)

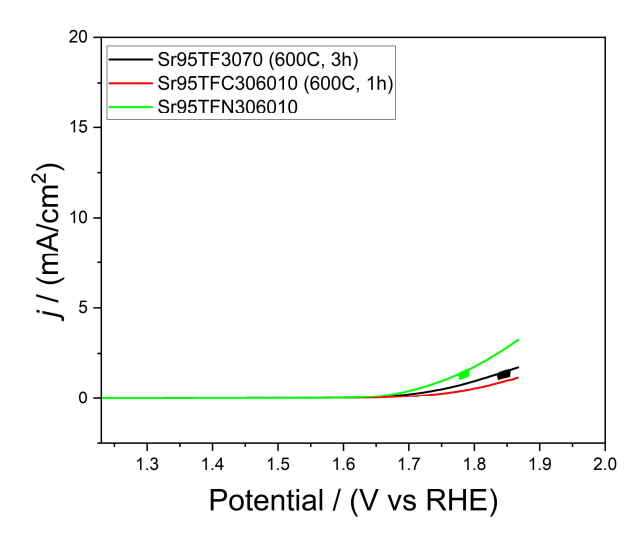


Figure 10: Current-voltage curves of a) BSCF-based catalysts and b) STFN-based catalysts. All measurements were conducted in a rotating disc electrode (RDE) configuration in a three-electrode





set up in 1 M KOH. A carbon rod and a saturated calomel electrode (SCE) were used as counter and reference electrodes, respectively. Scanning rate was 10 mV/s under continuous O₂ bubbling. The catalyst loading in all cases was 0.28 mg/cm² nominal RDE area.

Before electrochemical characterization, the RDE with as deposited catalyst was cleaned electrochemically by performing CV from 1.0 to 0.03 V vs. RHE at 50 mV s-1 until steady-state conditions were obtained. Subsequently, the catalyst was activated by CV at a scan rate of 10 mV/s from the non-Faradaic region to the potential required to reach a current density of 10 mA/cm². After 10 cycles of activation, most catalyst materials showed a steady-state behaviour.

From our initial screening with CV and LSV is apparent that the BSCF-based catalysts are superior to the STFN-based ones. Notice that the x- and y-axis scales in both current-voltage curves are the same.

The relatively modest performance of the STFN-based materials (0.09 mA/cm² at 400 mV overpotential for Sr95TF3070) can be attributed to multiple factors: the high-temperature processing required for phase formation leading to decreased surface area; the presence of secondary phases which not only may interfere with the electrochemistry but also indicate off-stoichiometry in the main perovskite phase; and the intrinsically lower OER activity of Fe compared to Co-based systems like BSCF. While this presents a challenging compromise between catalytic activity and the drive to eliminate toxic and scarce elements like Co, it also emphasizes the importance of developing lower-temperature synthesis routes and optimizing exsolution to maximize the activity of Co-free compositions.

According to the set targets, we aim at producing 50 mA/cm² at 400 mV overpotential, i.e. at 1.63 V vs RHE. Currently, the exsolved BSCF82-5AD produces 2.7 mA/cm² at 400 mV overpotential, while the Sr95TF3070 produces only 0.09 mA/cm² at 400 mV overpotential. Although these values are well below the set targets, there is still a lot of materials engineering to be conducted.

5 Conclusions

In conclusion, we have so far successfully synthesized a large number of BSCF- and STFM-based catalysts and it appears that the BSCF-based catalysts perform better than the STFN-based ones, and have good potential in reaching the set targets of REFINE. Nevertheless, the final selection will also depend on the "Materials Selection" and "LCA" analyses of WP14. Preliminary findings in this WP clearly indicate that STF-based catalysts score the highest in terms of environmental, economic and societal impact. What is also important to point out in the case of the BSCF-based catalysts is that Asite deficiency and reduction in Co content by 20% affect very little the electrochemical activity, which is a promising result in terms of material resources and Co reduction. While STFN-based materials currently show lower OER activity compared to BSCF counterparts, their Co-free composition offers a more sustainable pathway (currently also supported by our "Materials selection" study in WP14), and their performance could be significantly enhanced through ongoing development of low-temperature synthesis routes to achieve higher surface areas and better phase purity, alongside optimization of exsolution parameters to maximize active site density. Further optimization will be performed in both sets of catalysts and these will include the further tuning of the exsolution conditions (temperature, annealing conditions, time etc.), as well as the introduction of minimal amounts of noble metals, like Ru and Ir to boost the OER performance.





Disclaimer

"Funded by the European Union. Views and opinions expressed are however those of the author(s) only and do not necessarily reflect those of the European Union. Neither the European Union nor the granting authority can be held responsible for them."